Applied Surface Science 529 (2020) 147111

Contents lists available at ScienceDirect

Applied Surface Science

journal homepage: www.elsevier.com/locate/apsusc

Surface free energy analysis of ITO/Au/ITO multilayer thin films on polycarbonate substrate by apparent contact angle measurements

Salih Ozbay[a,*], Nursev Erdogan[b], Fuat Erden[c], Merve Ekmekcioglu[d,e], Mehtap Ozdemir[d], Gulnur Aygun[e], Lutfi Ozyuzer[d,e]

[a] Department of Chemical Engineering, Sivas University of Science and Technology, 58000 Sivas, Turkey
[b] Advanced Material, Process and Energy Technology Center, Turkish Aerospace, 06980 Ankara, Turkey
[c] Department of Aeronautical Engineering, Sivas University of Science and Technology, 58000 Sivas, Turkey
[d] Teknoma Technological Materials Inc., Izmir Technology Development Zone, Urla, 35430 Izmir, Turkey
[e] Department of Physics, Izmir Institute of Technology, Urla, 35430 Izmir, Turkey

ARTICLE INFO

Keywords:
Indium tin oxide
Gold
Polycarbonate
Contact angle
Surface free energy
Critical surface tension

ABSTRACT

A detailed surface free energy (SFE) knowledge of transparent conducting oxide (TCO)/metal/TCO electrodes is necessary for their applications related to surface wettability. However, SFE analysis of these surfaces has not been performed systematically previously. In this study, ITO and ITO/Au/ITO multilayer thin films were coated onto O_2 plasma treated polycarbonate (PC) substrates by magnetron sputtering. The wettability characteristics of untreated PC, O_2 plasma treated PC, ITO, Au interlayer, and ITO/Au/ITO multilayer thin films were evaluated by apparent contact angle measurements of nine different test liquids having various surface tensions. Following this, Lifshitz-van der Waals, acidic, basic, dispersive, and polar components of SFE were calculated using acid-base, geometric and harmonic mean approaches. In the present study, in which the significance of calculation methods and selected liquid pairs on SFE parameters were investigated, the effect of Au interlayer presence on SFE parameters were also evaluated simultaneously. The results showed that the total SFE values of ITO/Au/ITO multilayer thin films were found to be higher than that of ITO surface. The reasons behind this difference were discussed in terms of SFE components obtained using various liquid pairs by different methods. The results were also supported with XRD, XPS, AFM, and TEM analysis.

1. Introduction

Transparent conducting oxides (TCOs) such as Indium Tin Oxide (ITO), Indium Zinc Oxide (IZO) and Aluminum Zinc Oxide (AZO) have widespread applications in modern technologies thanks to their high optical transparency and electrical conductivity properties, as well as their stability in air [1,2]. ITO is one of the most widely used material among TCOs because there is a trade-off between optical transmittance and electrical conductance, and ITO offers a superior combination of them [3–6]. However, a single layer of ITO films is often inadequate to provide the desired electrical properties, and the incorporation of a thin conducting film between ITO layers without deteriorating the optical transparency is one of the easiest way to overcome this problem [2]. Au, Ag, Cu and Al are the most common metals which were used as an interlayer between bottom and top ITO layers for this purpose [7–10]. Among them, Au has been extensively preferred in many coatings due to its relatively lower electrical resistivity, higher optical transmittance, and atmospheric stability. Intensive efforts have been made to develop ITO/Au/ITO multilayer thin films on suitable substrates to be used in the optoelectronic research in recent years [7,9,11–18].

The wettability of an ITO surface [19] was proposed to be an important parameter in many applications, such as photovoltaic cells [20,21], light-emitting devices [22–28], semiconductor devices [29], nanorod films [30], and superhydrophobic coatings [31]. The control of the wettability, which is the ability of a surface to interact with a certain liquid, is relevant to many areas of technology [32,33]. For any material, the molecules in the bulk phase are surrounded by other molecules on every side resulting in a zero sum of net force, while the molecules at the surface encounter a net force called “surface free energy” (SFE) inward [32–34]. Unfortunately, the determination of the SFE for solids cannot be done by direct methods due to the low mobility of solid molecules, and the wettability that determined by contact angle measurements can be used as an indirect method for this purpose. The SFE components of a solid surface are critical for understanding,

* Corresponding author.
E-mail address: salihozbay@sivas.edu.tr (S. Ozbay).

https://doi.org/10.1016/j.apsusc.2020.147111
Received 14 May 2020; Received in revised form 20 June 2020; Accepted 28 June 2020
Available online 03 July 2020
0169-4332/

interpreting, and predicting many interface phenomena such as adsorption, wetting, adhesion, lubrication behavior, friction, and biocompatibility [32,35]. In many studies, the surface of an ITO has been modified to adapt to the specific application by altering the surface wettability [20–29,36,37]. For example, Besbes et al. treated the ITO surface with phosphonic acid to increase the SFE of the ITO and enhanced the ITO/polymer interface to be used in organic light-emitting devices [23]. Vunnam et al. treated the ITO surface with air plasma to attain a favorable interface between printed nano-inks and ITO surface, and obtained a desired interface by controlling the SFE of the ITO [37]. Similar studies showed that the oxygen treatment of the ITO surface to provide a higher SFE is one of the suitable treatment option for providing better adhesion with polymer substrates [19,22,38]. Dong et al. fabricated an inverted top-illuminated polymer solar cells by coating an ITO interlayer treated with UV-ozone on top of an Ag reflector to protect the Ag reflector from oxidation and to realize a hydrophilic surface without degrading the surface morphology or the optical reflectance [21]. Arazna et al. showed that the ultrasonic degreasing in acetone and ethyl alcohol is an effective way to increase the SFE of the ITO and might be useful in preparing ITO-based organic light emitting devices [27]. All of these results indicate that the SFE components of ITO and ITO/Au/ITO has an important role. However, the effect of Au interlayer on the SFE properties of ITO/Au/ITO multilayer thin films still remained elusive.

Besides, a contradiction is still present, of what would be the method of SFE calculation for an ITO surface. Some of the researchers used the acid-base approach [23,26,37,38], while others used the geometric [19,24,25,27,38] and harmonic mean approaches [22]. Elmas et al. used the equation of state approach to calculate the SFE values of the ITO on glass, PET and Si substrates by using water contact angle data [39]. Another case that cannot be explained is the effect of the selection of the liquid pairs used during calculations on the SFE components of an ITO surface. In fact, both the SFE calculation methods and the selection of liquid pairs are not only the problem of ITO but also of all solid surfaces. Intensive efforts have been made to calculate the SFE value of a solid surface thoroughly and to eliminate discrepancies in SFE calculations [40–49].

The main aim of this study is to reach a detailed SFE knowledge of the ITO-based films as accurately as possible by evaluating the wettability characteristics of ITO, Au interlayer (ITO/Au) and ITO/Au/ITO multilayer thin films by various SFE calculation methods. For this purpose, ITO, ITO/Au, and ITO/Au/ITO multilayer thin films were coated onto O_2 plasma treated polycarbonate (PC) substrates by magnetron sputtering. The O_2 plasma treated PC was used as substrate material in this study due to its adequate optical, mechanical and adhesion properties [50–53], and the SFE analysis of the untreated and O_2 plasma treated PC was also performed. Nine different test liquids having various surface tensions were used to prepare a comprehensive report, and the apparent contact angles of these liquids were measured on the prepared surfaces by the sessile drop method. Then, the dispersive and polar components of SFE were calculated using geometric (Owens and Wendt's method) [54] and harmonic (Wu's method) [55] mean approaches. The acidic and basic components of SFE were calculated using van Oss-Chaudhury-Good method [56]. Although calculation methods and selected liquid pairs were effective on SFE components, the total SFE of ITO/Au/ITO multilayer thin films were found to be higher than that of ITO surface by all methods. It was also observed that the duration of Au deposition had an important effect on the overall quality of the interlayer structure by changing the SFE values of Au interface. In addition, the critical surface tensions of ITO, ITO/Au and ITO/Au/ITO multilayer thin films were determined by Zisman's plot [57–60] to make clarify the effect of Au interlayer presence on the wettability properties of ITO-based films. The findings were also supported by various characterization methods such as XRD, XPS, AFM, and TEM.

2. Materials and methods

2.1. Materials

Polycarbonate (PC) was supplied from Makrolon (ASTM D1746, 50 mm × 50 mm × 21 mm). The ITO target was composed of In_2O_3 (90 wt%) and SnO_2 (10 wt%) with a thickness and diameter of 0.25 in. and 2 in., respectively. A high purity (99.99%) Au target was used with 0.125 in. thickness and 2 in. diameter. Ultrapure water (CAS Number: 7732-18-5), methanol (CAS Number: 67-56-1), formamide (CAS Number: 75-12-7), and diiodomethane (CAS Number: 75-11-6) were purchased from Merck. Glycerol (CAS Number: 56-81-5), ethylene glycol (CAS Number: 107-21-1), diethylene glycol (CAS Number: 111-46-6), 1-bromonaphthalene (CAS Number: 90-11-9), N,N-dimethylformamide (CAS Number: 68-12-2) and hexadecane (CAS Number: 544-76-3) were purchased from Sigma-Aldrich.

2.2. Preparation of ITO/Au/ITO multilayer thin films on polycarbonate

ITO and Au thin films were deposited on PC by magnetron sputtering as explained in our previous works [17,61]. Prior to deposition, the PC substrates were fully cleaned by ultrasonication in methanol and DI water for 20 min, and then dried under nitrogen atmosphere. PC substrates were also plasma-treated for 2 min under oxygen gas to increase surface hydrophilicity. A regular sputtering procedure initiated with evacuating the chamber below 2×10^{-6} Torr first, which was followed by a 5 min of pre-sputtering to remove the contaminants. Finally, the deposition was carried out at $\sim 3 \times 10^{-3}$ Torr, under pure Ar gas flow (40 sccm) and at room temperature in the absence of substrate heating. The deposition durations were 7.0 min for ITO layers and adjusted to 20 and 30 s for the Au to form a continuous interlayer. The sample preparation conditions, thickness and RMS roughness of the films are given in Supplementary Material Table S1.

2.3. XPS, AFM, XRD, and TEM analysis

A Veeco DEKTAK 150 profilometer was used to determine the thickness of the films and average values of 5 measurements taken from different locations were reported. X-Ray Photoelectron Spectroscopy (XPS) studies were conducted with an MXR1 Gun-400 μm 15 kV spectrometer equipped with an Al Kα source. The analyzed spot size was 400 μm with the analyzer pass energy of 300.0 eV. The binding energies were referenced to the neutral adventitious C1s peak at 284.6 eV. The RMS roughness of the surfaces were determined by using contact mode of AFM under ambient conditions on 10 μm × 10 μm surface areas. Grazing Incidence X-Ray Diffraction (GIXRD) was carried out in the Grazing focusing geometry at a grazing angle of the incident X-ray beam (ω) 0.75° using a Panalytical X-Ray Diffractometer, with Cu-Kα radiation (λ = 1.5406 Å). XRD patterns were recorded from 2θ = 20–70° with a step size of 0.016° for all samples. Cross sectional morphologies of films were analyzed using HRTEM analysis (Jeol, HRTEM). HRTEM samples were prepared by Focused Ion Beam (FIB) lithography.

2.4. Contact angle measurements and surface free energy calculations

The apparent contact angles (θ) under air were measured by the sessile drop method using Dataphysics (OCA 30) contact angle system. 5 μL drops of water (W), glycerol (GLY), formamide (FA), diiodomethane (DM), ethylene glycol (EG), diethylene glycol (DEG), 1-bromonaphthalane (BN), N,N-dimethylformamide (DF) and hexadecane (HD) were formed on the surfaces. Then, contact angles were determined after the needle was removed from the liquid droplet formed on the surface. The apparent contact angles were measured on at least ten different places of each surface for all of the test liquids on the surfaces and their mean values were calculated.

Table 1
Surface tensions (mJ/m^2) of the test liquids and apparent contact angle (°) results on untreated PC, O_2 plasma treated PC, ITO, ITO/Au, and ITO/Au/ITO surfaces.

Liquids	γ_{lv}	θ (°) Untreated PC	θ (°) Treated PC	θ (°) ITO	θ (°) ITO/Au (20 s)	θ (°) ITO/Au (30 s)	θ (°) ITO/Au (20 s)/ITO
W	72.8	82 ± 2	56 ± 2	90 ± 2	83 ± 1	79 ± 1	87 ± 1
GLY	64.0	74 ± 2	52 ± 2	87 ± 1	79 ± 1	76 ± 1	85 ± 1
FA	58.2	61 ± 2	32 ± 1	79 ± 2	61 ± 2	53 ± 1	71 ± 2
DM	50.8	32 ± 2	25 ± 2	54 ± 2	48 ± 2	46 ± 1	51 ± 2
EG	48.0	53 ± 2	46 ± 2	66 ± 2	63 ± 1	57 ± 1	65 ± 1
DEG	44.4	49 ± 1	36 ± 1	63 ± 1	58 ± 1	51 ± 2	62 ± 2
BN	44.4	27 ± 1	20 ± 1	46 ± 2	37 ± 1	36 ± 2	44 ± 1
DF	37.1	25 ± 2	8 ± 1	36 ± 2	19 ± 1	14 ± 1	33 ± 2
HD	27.5	Spreading	Spreading	20 ± 2	Spreading	Spreading	17 ± 1

W: Water, GLY: Glycerol, FA: Formamide, DM: Diiodomethane, EG: Ethylene glycol, DEG: Diethylene glycol, BN: 1-Bromonaphthalene, DF: N,N-dimethylformamide, HD: Hexadecane.

The critical surface tension (γ_c) values of the coatings were determined by Fox and Zisman's method [57–60]. The contact angle measurement results of liquid drops having various surface tension (γ_{LV}) values were used to plot the cos θ values against γ_{LV}. The surface tensions of these liquids were obtained from the literature [32,35,62,63], and given in Table 1. The equation used for determining the critical surface tension is written as,

$$\cos\theta = 1 - \beta(\gamma_{LV} - \gamma_c) \quad (1)$$

where the slope of the line gives -β, and the intercept gives ($\beta\gamma_c$ + 1). The γ_c was calculated by using the slope and intercept values of the Zisman's plot [32,33].

The dispersive (γ_{SV}^d) and polar (γ_{SV}^p) components of the SFE were calculated by applying geometric (Owens and Wendt's method) [54] and harmonic (Wu's method) [55] mean approaches. The equation of the geometric mean approach can be written as,

$$\gamma_{LV}(1 + \cos\theta) = 2\left(\sqrt{\gamma_{SV}^d \gamma_{LV}^d} + \sqrt{\gamma_{SV}^p \gamma_{LV}^p}\right) \quad (2)$$

The equation of the harmonic mean approach can be written as,

$$\gamma_{LV}(1 + \cos\theta) = 4\left(\frac{\gamma_{SV}^d \gamma_{LV}^d}{\gamma_{SV}^d + \gamma_{LV}^d} + \frac{\gamma_{SV}^p \gamma_{LV}^p}{\gamma_{SV}^p + \gamma_{LV}^p}\right) \quad (3)$$

By solving the equation (2) for the geometric mean approach and equation (3) for the harmonic mean approach, γ_{SV}^d and γ_{SV}^p components of the SFE were found. The γ_{LV}^d and γ_{LV}^p values of the liquids used in these equations were retrieved from the literature [32,34] and given in Supplementary Material Table S2. Then, the total SFE (γ_S^{Tot}) of the surface was calculated as,

$$\gamma_S^{Tot} = \gamma_{SV}^d + \gamma_{SV}^p \quad (4)$$

Lifshitz-van der Waals and acid-base interaction parameters of the SFE were calculated by applying acid-base (van Oss-Chaudhury-Good method) approach [56]. Contact angles of W, GLY, EG, FA, DM and BN liquid drops were measured on the sample surfaces for this purpose. The main equation of the van Oss-Chaudhury-Good method is written as,

$$\gamma_{LV}(1 + \cos\theta) = 2\left(\sqrt{\gamma_S^{LW}\gamma_L^{LW}} + \sqrt{\gamma_S^+\gamma_L^-} + \sqrt{\gamma_S^-\gamma_L^+}\right) \quad (5)$$

where S denotes solid; L liquid; V vapor and γ_S^{LW} is the Lifshitz-van der Waals SFE term which comprises "dispersion", "dipolar" and "induction" interactions. The surface tension components of the liquids used in van Oss-Chaudhury-Good method were obtained from the literature [32,62–64], and given in Supplementary Material Table S3. Other equations are,

$$\gamma_S^{AB} = 2\sqrt{\gamma_S^+\gamma_S^-} \quad (6)$$

$$\gamma_S^{Tot} = \gamma_S^{LW} + \gamma_S^{AB} \quad (7)$$

where γ_S^+ denotes Lewis acid parameter, γ_S^- denotes Lewis base parameter and γ_S^{AB} comprises all the electron donor–acceptor (acid-base) interactions. γ_S^{LW} was calculated by using θ results of DM and BN liquids, and then W-GLY, W-EG, W-FA θ pairs were used to calculate γ_S^+ and γ_S^- values [32,33,56].

3. Results and discussion

3.1. Characterization, wettability properties and surface free energy analysis of untreated and O_2 plasma treated polycarbonate substrates

Plasma treatment is one of the most popular surface modification methods used to increase adhesion strength between substrate and coating by improving surface hydrophilicity [50,53,65]. Contact angle results on PC surfaces that were untreated and O_2 plasma treated are given in Table 1. The W contact angle value of untreated PC was measured as 82°, indicating relatively poor wettability. A significant reduction in the contact angle results for all test liquids was observed after O_2 plasma treatment of the PC. The work of adhesion (W_a) is closely related to the effectiveness of polar functional groups on the polymer surface treated by O_2 plasma [66]. We calculated the W_a with Young-Dupre equation [$W_a = \gamma_{lv}(1 + cos\theta)$] for polar test liquids. W_a values for W-PC interface increased sharply from 82.9 mJ/m^2 to 113.5 mJ/m^2 with O_2 plasma treatment as given in Fig. 1, indicating that the presence of considerable amount of polar functional groups on the surface. Similar trends were also observed for GLY, FA and EG liquids which are given in Fig. 1. The oleophobic behavior of the PC surfaces were evaluated by measuring the contact angles of HD liquid which is the commonly accepted index of oleophobicity [67]. HD droplets were spread on the both untreated and O_2 plasma treated PC surfaces due to the strong liquid/solid interaction, indicating that PC surfaces were very oleophilic.

SFE components of the untreated and O_2 plasma treated PC

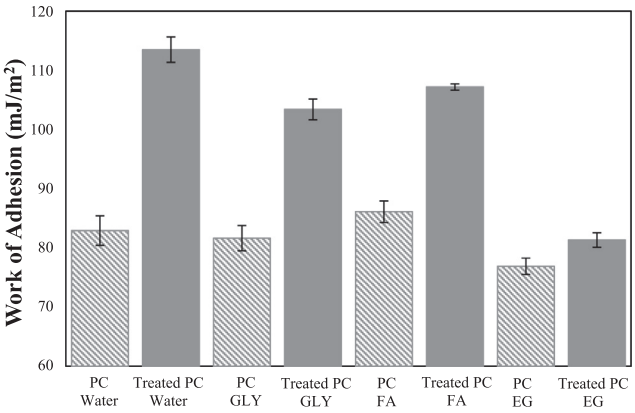

Fig. 1. Work of adhesion values of PC and O_2 plasma treated PC. GLY, glycerol; FA, formamide; EG, ethylene glycol.

Table 2
Values of the Lifshitz-van der Waals, acidic and basic components (mJ/m^2) of the PC and O_2 plasma treated PC surfaces calculated by van Oss-Chaudhury-Good method.

Liquid pairs	PC					O_2 plasma treated PC				
	γ_s^{LW}	γ_s^+	γ_s^-	γ_s^{AB}	γ_s^{Tot}	γ_s^{LW}	γ_s^+	γ_s^-	γ_s^{AB}	γ_s^{Tot}
W-FA-DM	43.37	0.00	5.70	0.00	43.37	46.15	0.59	17.54	6.45	52.60
W-EG-DM	43.37	0.00	4.47	0.03	43.40	46.15	0.00	29.88	0.00	46.15
W-GLY-DM	43.37	0.00	5.96	0.00	43.37	46.15	0.16	20.72	3.70	49.85
W-FA-BN	39.69	0.00	5.58	0.11	39.80	41.76	1.22	17.29	9.19	50.96
W-EG-BN	39.69	0.05	4.69	0.96	40.65	41.76	0.00	30.52	0.00	41.76
W-GLY-BN	39.69	0.00	6.25	0.00	39.69	41.76	0.41	21.35	5.94	47.70
mean	41.53	0.01	5.44	0.18	41.72	43.96	0.40	22.88	4.21	48.17

substrates were calculated with van Oss-Chaudhury-Good method using θ results for W, DM, BN, FA, EG and GLY drops. DM and BN were chosen as the nonpolar liquids, and W-FA, W-EG and W-GLY were selected as the polar liquids in evaluating the SFE components using the three-liquid acid-base method [56]. Some of the liquid pair combinations (e.g. GLY-FA-DM/BN and GLY-EG-DM/BN) were deviated quite a lot thus excluded from the SFE calculations. In fact, incompatibilities associated with the use of GLY-FA and GLY-EG liquid pairs in SFE calculations were already determined by Della Volpe et al. [46,48]. The results obtained for PC surfaces by using these different liquid combinations are given in Table 2. As expected, the selection of the liquid pairs affected the results of the SFE components. For example, the acid-base component (γ_S^{AB}) of the SFE was found as 0 mJ/m^2 with W-EG-DM and W-EG-BN triples for O_2 plasma treated PC surface, indicating that the γ_S^{Tot} is mainly due to dispersive character. However, the γ_S^{AB} was found as 6.45 mJ/m^2 and 9.19 mJ/m^2 with W-FA-DM and W-FA-BN triples respectively for the same surface, indicating that the O_2 plasma treated PC surface is bipolar and has a significant polarity. These results show that calculating the SFE parameters using average data of various liquid pairs will result in more consistent evaluations. When all well-conditioned liquid pairs are considered, the average values for γ_S^{Tot}, for γ_S^{AB}, and for γ_S^{LW} on the untreated PC surface were calculated as 41.72, 0.18, and 41.53 mJ/m^2, respectively. Whereas, the average values for γ_S^{Tot}, for γ_S^{AB}, and for γ_S^{LW} on the O_2 plasma treated PC surface were calculated as 48.17, 4.21, and 43.96 mJ/m^2, respectively. According to the calculations, all the SFE components of O_2 plasma treated PC surface were found to be higher than that of untreated PC surface. The γ_S^{AB} shows the polar contribution of the SFE and the increase in this parameter were much higher than the increase in γ_S^{LW}. This indicates strong interaction between polar liquid droplets and O_2 plasma treated PC surface. On the other hand, the γ_S^- component of the SFE shows the hydrogen bonding ability of the carbonyl groups that were present on the surface [68], and the O_2 plasma treatment of the PC surface was found to be very effective for increasing the γ_S^- component, while the γ_S^+ of the surface only increased slightly. The average value for the γ_S^- on PC surface increased from 5.44 to 22.88 mJ/m^2 with the O_2 plasma treatment, suggesting that the carbonyl groups capable of hydrogen bonding covered most of the polymer surface following the plasma treatment. These results show that O_2 plasma treatment of the PC surface is effective for increasing the SFE and hydrophilicity by forming of new oxygenated groups on the surface [51,52,69,70].

XPS analysis was carried out on untreated and O_2 plasma treated PC surface to identify the changes in intensity of chemical bindings. XPS survey spectra, O1s and C1s core spectra of untreated and O_2 plasma treated PC are given in Supplementary Material Fig. S1. XPS survey analysis of the PC depicted in Fig. S1(a) revealed that there are only C and O elements on the PC surface. Elemental percentage composition of the untreated PC was 96.71% for C and 3.29% for O. The O percentage value on PC surface increased from 3.29 to 12.52% with the O_2 plasma treatment due to oxidation of the groups on the PC surface. A remarkable change in the position and relative height of the peaks was observed in the spectrum of treated PC with respect to the spectrum of the untreated PC as given in Fig. S1(b). The increase in SFE and change in wettability properties by plasma treatment can be attributed to the increasing the intensity of –(O = C)–O– by insertion of new polar groups to the PC surface as shown in Fig. S1(c) [51]. Although oxidation of the surface has been demonstrated, the material's wettability response cannot be ascribed only to this chemical change. Thus, a joint morphological and chemical effect should be studied where the structure and morphology play the dominant role. Topography is one of the most important physical characteristics of surfaces, which influence their wettability properties. The surface topography of the untreated and O_2 plasma treated PC were determined by AFM analysis and given in Fig. 2. RMS roughness were measured as 1.28 ± 0.53 nm for untreated PC and as 1.35 ± 0.40 nm for O_2 plasma treated PC surface. These results were very close to each other indicating that effects of O_2 plasma treatment are homogenous all over the surface, and SFE differences between treated and untreated PC were mainly originated from chemical modification of PC surface with O_2 plasma treatment.

The dispersive γ_S^d and polar γ_S^p components of the SFE for PC were also calculated using geometric and harmonic mean approaches and the results are given in Supplementary Material Tables S4 and S5. The average values for γ_S^{Tot}, for γ_S^p, and for γ_S^d on untreated PC surface were calculated as 42.57, 1.03, and 41.53 mJ/m^2, respectively by using geometric mean approach. Whereas, the average values for γ_S^{Tot}, for γ_S^p, and for γ_S^d on O_2 plasma treated PC surface were calculated as 50.97, 7.01, and 43.96 mJ/m^2, respectively. These values are close to those obtained from van Oss-Chaudhury-Good method. However, when using harmonic mean approach, the γ_S^p components of the SFE were found to be higher than the results obtained with Owens-Wendt and van Oss-Chaudhury-Good method. For example, the average value for the γ_S^p was calculated as 3.24 mJ/m^2 for untreated PC surface and as 9.99 mJ/m^2 for O_2 plasma treated PC surface by using the harmonic mean approach. Using the same method, the average value for the γ_S^{Tot} was calculated as 44.96 mJ/m^2 for untreated PC surface and as 54.02 mJ/m^2 for O_2 plasma treated PC surface. In agreement with our results, Wu has shown that the SFE parameters calculated by the harmonic mean method are higher than the geometric mean approach [55].

3.2. Characterization, wettability properties and surface free energy analysis of ITO/Au/ITO multilayer thin films

The prepared surfaces were smooth and gave reproducible contact angle results. The contact angle results of the nine different test liquids on ITO, Au coated ITO (ITO/Au) and ITO/Au/ITO surfaces are given in Table 1. These results are in good agreement with the previous reports. For example, Besbes et al. [23] reported θ_{water} = 92 ± 1.5°, Devenas et al. [26] reported θ_{water} = 92°, You and Dong [24] reported θ_{water} = 85.1° for an untreated ITO surface, and we measured θ_{water} = 90 ± 2° for our prepared ITO surface. The contact angle results shown in Table 1 indicate clearly that the presence of Au interlayer between ITO layers have a profound influence on the contact

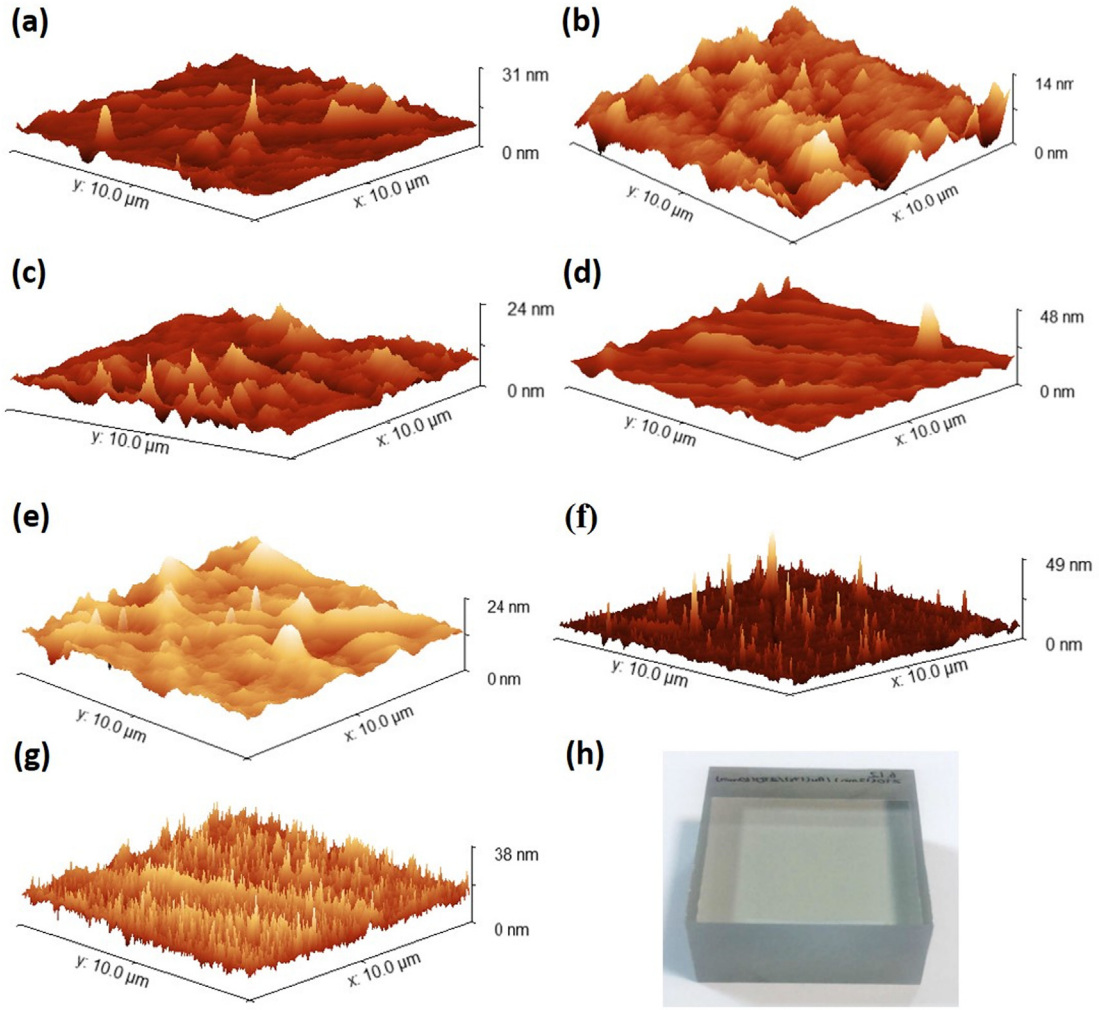

Fig. 2. 3D AFM images of (a) PC, (b) Plasma-treated PC, (c) ITO, (d) ITO/ITO (e) ITO/Au (20 s), (f) ITO/Au (30 s), (g) ITO/Au (20 s)/ITO and (h) photographic image of ITO/Au (20 s)/ITO.

angles of the thin films formed. The surface topography of the samples was determined by AFM and given in Fig. 2. RMS roughness values was found to be 1.73 ± 0.54 nm for the ITO surface, and 3.39 ± 0.60 nm for the ITO/Au/ITO surface. Deposition of single and double layers of ITO without Au interlayer resulted in a gradual improvement of RMS roughness as can be seen in Fig. 2(c) and (d). Likewise, a similar trend was observed upon increasing the deposition duration of Au from 20 to 30 s as shown in Fig. 2(e) and (f). Although, one might expect a less increase of roughness with a smaller change of Au thickness comparing to ITO, a similar increasing trend may be related to the delamination of layer. Moreover, the highest RMS roughness was obtained with the insertion of top ITO layer assembling ITO/Au (20 s)/ITO as depicted in Fig. 2(g). Besides, photographic image of the multilayer film of the ITO/Au (20 s)/ITO is shown in Fig. 2(h). The nearly zero nanoscale roughness values of ITO and ITO/Au/ITO surfaces indicate that all surfaces were quite smooth. Yet, the contact angle differences between ITO and ITO/Au/ITO might still have been slightly affected by the presence of minimal roughness. Besides, preferred orientation of ITO top layer through the (400) plane is effective on the contact angle results. It was found that the contact angle results of the ITO/Au/ITO surface were lower than that of the ITO surface for all test liquids. The reasons under this difference will be discussed with XRD analysis. In general, if W contact angle is less than 90°, the surface is hydrophilic, however if W contact angle is greater than 90°, it means that the surface is hydrophobic [32]. The W contact angle was found as 90° for ITO film and 87° for ITO/Au/ITO film, indicating that ITO surfaces were close to the limit of hydrophobic/hydrophilic balance. The oleophobic behavior of the ITO surfaces were evaluated by measuring the contact angle of HD liquid. The HD contact angle was found as 20° for ITO film and 17° for ITO/Au/ITO film, indicating that ITO surfaces were oleophilic. However, the HD droplets were spread on the ITO/Au surface, indicating that the Au/HD adhesion were much stronger than the cohesion within the HD molecules [33].

Fig. 3 shows the XRD patterns of single and bilayer ITO and multilayer ITO/Au (20 s)/ITO thin films onto PC. Peaks found at 29.85° ± 0.1 and 34.85° ± 0.1 can be indexed to the (222) and (400) planes of ITO with bixbyite crystal structure (JCPDS File No. 89-4596). No peak belonging to SnO or SnO_2 was detected. The existence of both (400) and (222) family of planes indicates the polycrystalline nature of the films that were grown in the absence of substrate heating. XRD pattern of single ITO film has a very low crystallinity as seen in Fig. 3(a). This is mainly due to room temperature deposition and low thickness of the film. Hence, XRD analysis of ITO double coating was conducted to examine the variation of crystal properties without Au interlayer. As shown in Fig. 3(b), intensity of the peaks increased with thickness by forming ITO/ITO as compared to single layer ITO. Yet, the crystal orientation in [111] direction was observed in both single and bilayer ITO. It is seen in Fig. 3 (c) that Au (111) peak is obvious at 38.25° in the multilayered ITO/Au (20 s)/ITO (JCPDS File No. 04-0784). By the insertion of Au interlayer, ITO top layer of the multilayer film is found to be oriented through [100] direction. While ITO films deposited by various techniques are often reported to orient in [111]

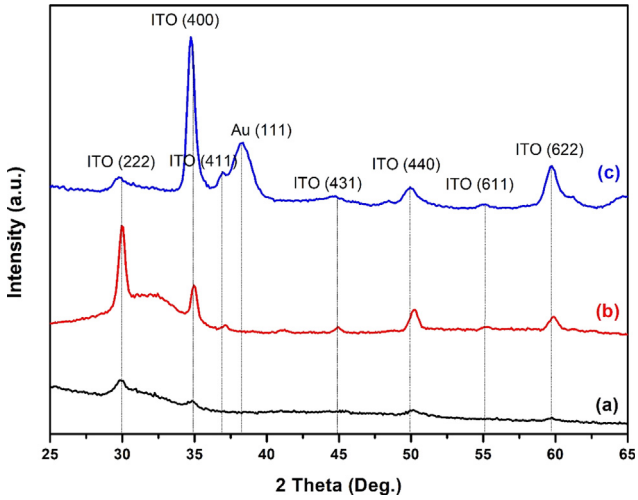

Fig. 3. XRD patterns of (a) ITO, (b) ITO/ITO and (c) ITO/Au (20 s)/ITO on PC substrate.

Table 3
Values of the Lifshitz-van der Waals, acidic and basic components (mJ/m^2) of the ITO, ITO/Au and ITO/Au/ITO surfaces calculated by van Oss-Chaudhury-Good method.

Sample	Liquid pairs	γ_s^{LW}	γ_s^+	γ_s^-	γ_s^{AB}	γ_s^{Tot}
ITO	W-FA-DM	32.02	0.00	7.66	0.00	32.02
	W-EG-DM	32.02	0.01	3.52	0.38	32.40
	W-GLY-DM	32.02	0.00	6.52	0.00	32.02
	W-FA-BN	31.88	0.00	7.66	0.00	31.88
	W-EG-BN	31.88	0.01	3.53	0.41	32.29
	W-GLY-BN	31.88	0.00	6.54	0.00	31.88
	mean	31.95	0.00	5.90	0.13	32.08
ITO/Au (20 s)	W-FA-DM	35.38	0.18	4.70	1.82	37.20
	W-EG-DM	35.38	0.00	7.39	0.00	35.38
	W-GLY-DM	35.38	0.00	8.36	0.00	35.38
	W-FA-BN	35.91	0.14	4.71	1.63	37.54
	W-EG-BN	35.91	0.00	7.35	0.00	35.91
	W-GLY-BN	35.91	0.00	8.30	0.00	35.91
	mean	35.65	0.05	6.80	0.57	36.22
ITO/Au (20 s)/ITO	W-FA-DM	33.71	0.00	6.06	0.00	33.71
	W-EG-DM	33.71	0.00	5.08	0.00	33.71
	W-GLY-DM	33.71	0.00	8.03	0.00	33.71
	W-FA-BN	32.81	0.00	6.02	0.00	32.81
	W-EG-BN	32.81	0.00	5.14	0.10	32.92
	W-GLY-BN	32.81	0.00	8.13	0.00	32.81
	mean	33.26	0.00	6.41	0.05	33.31

direction, a preferred orientation along (400) plane was already reported in ITO/Au/ITO multilayer films on PC substrate due to Au interlayer [17]. Hence, once the (400) plane-oriented crystals are formed on the Au interlayer, the film would grow preferentially using the initially formed (400) plane-oriented crystals [71]. Furthermore, the crystallinity of ITO is enhanced by inserting Au interlayer due to nucleation seed effect of interlayer as shown in Fig. 3.

The SFE results obtained for ITO, ITO/Au, and ITO/Au/ITO surfaces by using six different liquid combinations are given in Table 3. It is clearly seen that the van Oss-Chaudhury-Good method provides similar γ_S^{Tot} values for the same ITO surface even if the liquid pair used is changed. For example, by using the W-FA-DM and W-GLY-DM, the γ_S^{Tot} of ITO film was found as 32.02 mJ/m^2 and this value vas very close to 31.88 mJ/m^2 which was found by using W-FA-BN and W-GLY-BN liquid triples. Similarly, the γ_S^{Tot} values of ITO/Au/ITO film were calculated as 33.71 mJ/m^2 using all liquid triples containing DM. Although van Oss-Chaudhury-Good methodology was successful for determining the SFE components of the surfaces, sometimes negative values can be seen in the square roots of γ_S^+ and γ_S^- [33,64]. The negative values of square roots of γ_S^+ and γ_S^- were encountered in our work, and we assumed these values zero as advised by Robert J. Good [64]. Accordingly, this caused γ_S^{AB} to be calculated as zero. Thus, the contribution to the γ_S^{Tot} was only originated from the γ_S^{LW}. Since the γ_S^{AB} shows the polar contribution of the SFE, hence, it is difficult to analyze polar interactions of ITO surface with this method [38]. However, van Oss-Chaudhury-Good method gives useful information on the acidity and basicity of the surfaces in terms of γ_S^+ and γ_S^- as given in Table 3. It is clearly seen that all the ITO surfaces are on the average monopolar basic because γ_S^+ values were found to be quite small compared with the γ_S^- component.

The dispersive γ_S^d and polar γ_S^p components of the SFE for ITO surfaces were calculated using geometric and harmonic mean approaches and the results are given in Tables 4 and 5. The average values for γ_S^{Tot}, for γ_S^p, and for γ_S^d on the ITO surface were calculated as 32.59, 0.64, and 31.95 mJ/m^2, respectively by using geometric mean approach. Whereas, the average values for γ_S^{Tot}, for γ_S^p, and for γ_S^d on the ITO/Au/ITO surface were calculated as 34.11, 0.85, and 33.26 mJ/m^2, respectively. According to the calculations, all the SFE components of ITO/Au/ITO surface were found to be higher than that of ITO surface, indicating that the presence of Au interlayer resulted in an increase of the SFE components. In order to explain this situation, the SFE components of the Au interlayer were determined. The average values for γ_S^{Tot}, for γ_S^p, and for γ_S^d on the Au interlayer coated in 20 s were calculated as 37.09, 1.45, and 35.65 mJ/m^2, respectively by using the geometric mean approach, indicating that the SFE components of the Au interlayer were quite higher than the both ITO and ITO/Au/ITO surfaces as shown in Fig. 4. These results suggest that Au interlayer that have higher SFE between ITO layers in thin films could interact with liquids which located over the outer layer. Similar trend was also observed by using harmonic mean approach as given in Table 5.

In addition, the effect of Au deposition time on the overall quality of the sandwich films was also evaluated. When the Au deposition time adjusted to 20 s, the thickness of Au interlayer was 10 nm as can be seen from the cross section TEM image in Fig. 5(a) and (b). Besides, ITO/Au

Table 4
Surface free energy components (mJ/m^2) of the ITO, ITO/Au and ITO/Au/ITO surfaces calculated by geometric mean approach.

Liquid Pairs	ITO			ITO/Au (20 s)			ITO/Au (20 s)/ITO		
	γ_s^d	γ_s^p	γ_s^{Tot}	γ_s^d	γ_s^p	γ_s^{Tot}	γ_s^d	γ_s^p	γ_s^{Tot}
W-DM	32.02	1.95	33.97	35.38	3.35	38.73	33.71	2.46	36.17
W-BN	31.88	1.98	33.85	35.91	3.24	39.15	32.81	2.62	35.43
FA-DM	32.02	0.00	32.02	35.38	1.81	37.20	33.71	0.23	33.95
FA-BN	31.88	0.00	31.88	35.91	1.64	37.55	32.81	0.35	33.17
EG-DM	32.02	0.57	32.59	35.38	0.43	35.81	33.71	0.43	34.15
EG-BN	31.88	0.59	32.47	35.91	0.36	36.27	32.81	0.57	33.38
GLY-DM	32.02	0.02	32.03	35.38	0.39	35.77	33.71	0.03	33.74
GLY-BN	31.88	0.02	31.90	35.91	0.33	36.24	32.81	0.06	32.88
mean	31.95	0.64	32.59	35.65	1.45	37.09	33.26	0.85	34.11

Table 5
Surface free energy components (mJ/m^2) of the ITO, ITO/Au, and ITO/Au/ITO surfaces calculated by harmonic mean approach.

Liquid pairs	ITO			ITO/Au (20 s)			ITO/Au (20 s)/ITO		
	γ_s^d	γ_s^p	γ_s^{Tot}	γ_s^d	γ_s^p	γ_s^{Tot}	γ_s^d	γ_s^p	γ_s^{Tot}
W-DM	33.44	5.55	38.99	36.38	7.83	44.21	34.91	6.46	41.37
W-BN	32.64	5.70	38.34	36.28	7.85	44.12	33.47	6.74	40.21
FA-DM	33.44	0.00	33.44	36.38	3.11	39.49	34.91	0.79	35.70
FA-BN	32.64	0.00	32.64	36.28	3.15	39.42	33.47	1.25	34.72
EG-DM	33.44	1.45	34.89	36.38	1.41	37.79	34.91	1.31	36.23
EG-BN	32.64	1.66	34.30	36.28	1.43	37.71	33.47	1.67	35.14
GLY-DM	33.44	0.00	33.44	36.38	1.56	37.93	34.91	0.17	35.08
GLY-BN	32.64	0.19	32.82	36.28	1.58	37.86	33.47	0.54	34.01
mean	33.04	1.82	34.86	36.33	3.49	39.82	34.19	2.36	36.56

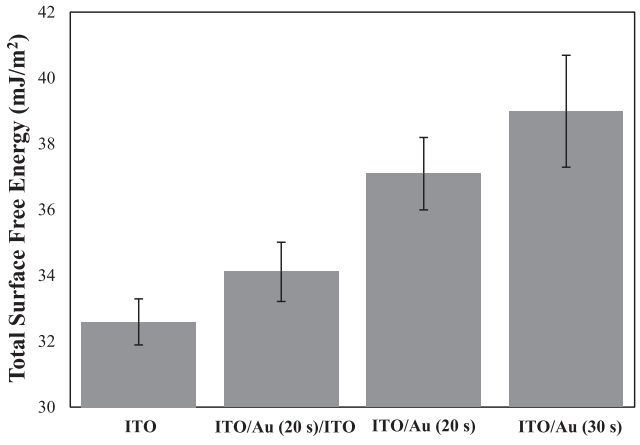

Fig. 4. Comparison of total surface free energy values of ITO, ITO/Au, and ITO/Au (20 s)/ITO surfaces calculated by geometric mean approach.

(20 s)/ITO exhibited a smooth and uniform thickness without any observable defects as depicted in Fig. 5(b). As the deposition time of Au increases, interlayer Au film is no longer stands on the bottom ITO layer as shown in Fig. 5(c). Furthermore, once the top layer is deposited, multilayer film is delaminated entirely, even the bottom ITO layer still adheres to the surface as seen in Fig. 5(d). Delamination is probably resulted by the thickening of Au interlayer which was measured as 15 nm. These observations are in good accordance with the SFE results in Tables S6 and S7 in the Supplementary Material file. The average values of γ_S^{Tot}, γ_S^p, and γ_S^d for the 30 s coated Au interlayer were calculated as 38.99, 2.59, and 36.40 mJ/m^2, respectively by using the geometric mean approach. This indicates that the SFE components of Au interlayer that have 15 nm thick were higher than that of the Au interlayer that have 10 nm thick as shown in Fig. 4. On the other hand, it was found that the SFE components of the thinner Au interlayer (10 nm) were relatively closer to the SFE components of bottom ITO layer. Therefore, when the Au deposition time was further increased, the difference between the SFE components of ITO and Au interlayer extended. This might be the reason for the delamination of Au

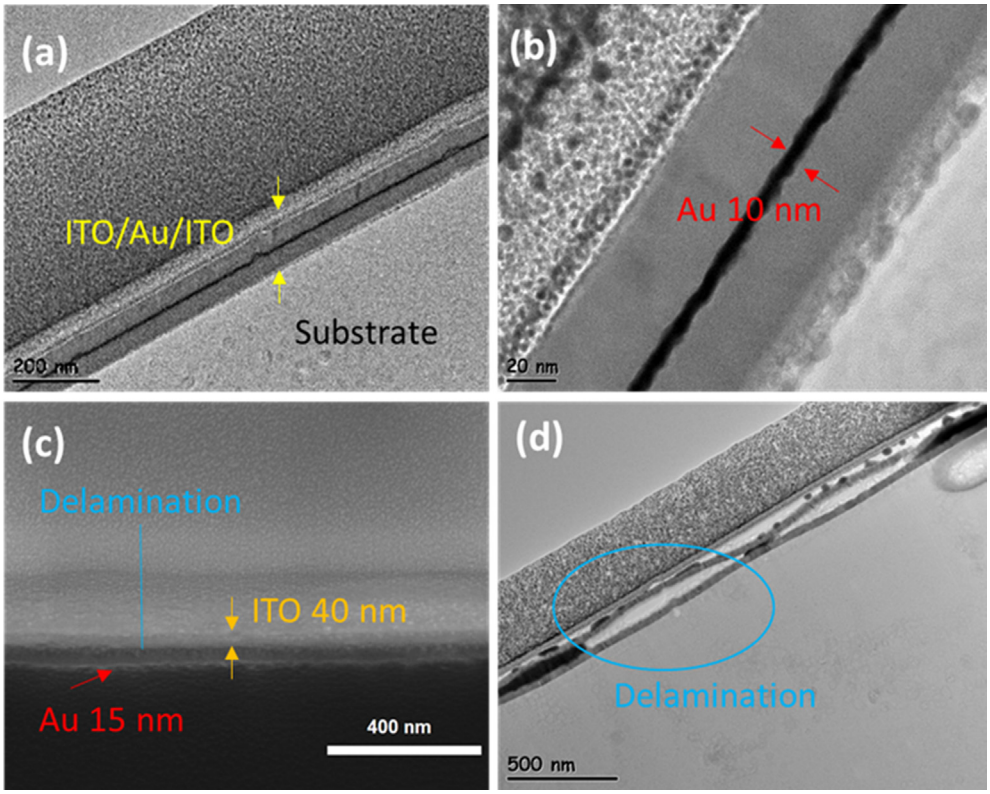

Fig. 5. Cross section HRTEM images of ITO/Au (20 s)/ITO with (a) Low magnification and (b) high magnification, (c) FESEM image of ITO/Au (30 s) and (d) HRTEM image of ITO/Au (30 s)/ITO.

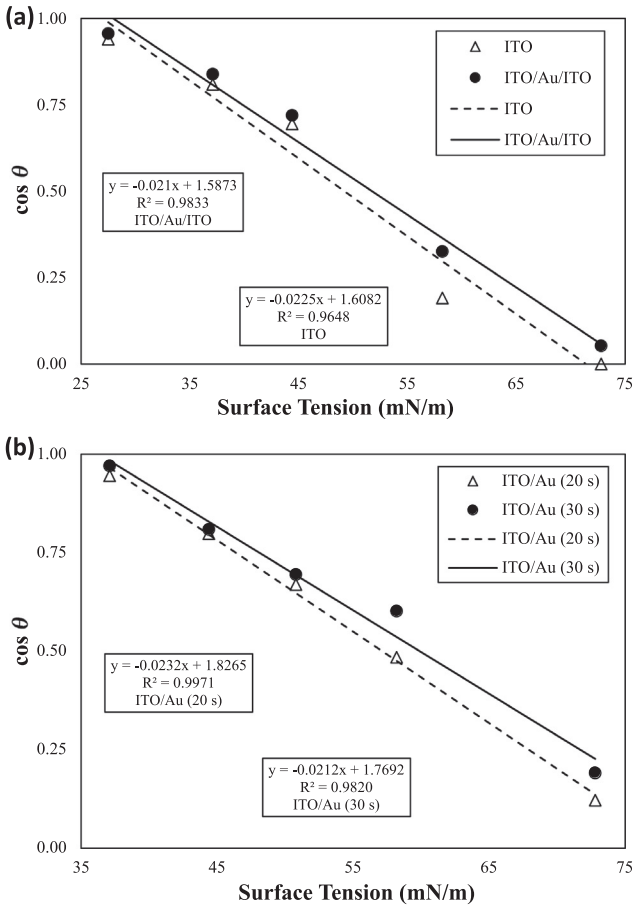

Fig. 6. Cosine of the contact angle versus surface tension for (a) ITO, ITO/Au (20 s)/ITO (b) ITO/Au surfaces.

interlayer when it deposited for 30 s. Regarding the thickness of bottom ITO layer, it was found about 40 nm in Fig. 5(c). Overall, the thickness values were in fairly good agreement with the actual measurement results by surface profilometer as given in Table S1.

Finally, the critical surface tensions (γ_c) of the ITO, ITO/Au and ITO/Au/ITO surfaces were determined from the Zisman's plots using contact angle results and surface tension values of the test liquids. The cos θ against γ_{LV} values were plotted in a coordination system to construct Zisman charts as shown in Fig. 6. It may not always be possible to obtain plots with high regression coefficient values in Zisman's plots [60]. When the results of all nine liquids used in the Zisman's drawings, R^2 values were found to be lower than 0.9. However, it should be close to 1 for better estimation of the γ_c. Thus, most suitable liquids were selected to provide graphs with better regression coefficient values. We used W, FA, BN, DF, and HD liquids for the ITO surfaces, and W, FA, DM, BN, DF liquids selected for the Au surfaces. Then, the regression coefficient values between 0.96 and 0.99 were found as given in Fig. 6. The γ_c value of the ITO surfaces were found as 27.0 mJ/m^2 for the ITO single layer surface and as 28.0 mJ/m^2 for the ITO/Au/ITO surface. Whereas, the γ_c value of the Au interlayer was found as 35.6 mJ/m^2 and 36.3 mJ/m^2 for 20 and 30 s Au deposition durations respectively, indicating that the γ_c of the Au interlayer were quite higher than the both ITO and ITO/Au/ITO surfaces. Another observation is that the γ_c value of the surfaces were found to be lower than the SFE results obtained with Owens-Wendt and van Oss-Chaudhury-Good method. This could be understandable as the values of γ_c differ depending on the liquid series used in the calculations. In addition, Zisman warned that γ_c and γ_{SV} are not equal and γ_c is only an empirical value characteristic of a given solid, while γ_{SV} is a thermodynamic quantity [32,57–59].

4. Conclusions

In this work, ITO and ITO/Au/ITO multilayer thin films were deposited onto O_2 plasma treated PC by magnetron sputtering. SFE components of the untreated PC, O_2 plasma treated PC, ITO, ITO/Au, and ITO/Au/ITO multilayer thin films were determined by acid-base, geometric mean and harmonic mean approaches using various liquid combinations. It was found that the calculation methods and selected liquid pairs affect the SFE values for the same surface significantly. Our results indicate that acid-base approach and geometric mean approach give similar γ_S^{Tot} values when the mean value of liquid combinations take into consideration. The negative values of square roots of γ_S^+ and γ_S^- were encountered for ITO and ITO/Au/ITO surfaces, and this caused the γ_S^{AB} to be calculated as zero. This indicated that it is difficult to analyze the contribution of polar interactions to the total SFE for an ITO surface with acid-base method. Harmonic mean approach provided slightly higher SFE values for all of the surfaces examined as compared to the geometric mean and acid-base approaches. While the acid-base approach is still useful for observing the acidity and basicity of an ITO surface, the geometric and harmonic mean approaches are suggested to determine the polar component of SFE. On the other hand, O_2 plasma treatment of the PC is effective for making the surface of PC compatible with an ITO coating by increasing the SFE values of the PC. The SFE components of ITO/Au/ITO surface were found to be higher than that of single ITO layer due to the presence of Au interlayer, which possess a higher SFE than ITO. The necessity of using the mean data of many liquid pairs in calculating the SFE components of similar surfaces for making a reliable evaluation has been seen.

CRediT authorship contribution statement

Salih Ozbay: Conceptualization, Methodology, Formal analysis, Investigation, Visualization, Writing - original draft, Writing - review & editing, Supervision. **Nursev Erdogan:** Software, Formal analysis, Investigation, Visualization, Writing - review & editing. **Fuat Erden:** Visualization, Writing - review & editing. **Merve Ekmekcioglu:** Investigation. **Mehtap Ozdemir:** Writing - review & editing. **Gulnur Aygun:** Resources, Writing - review & editing. **Lutfi Ozyuzer:** Resources, Writing - review & editing.

Declaration of Competing Interest

The authors declare that they have no known competing financial interests or personal relationships that could have appeared to influence the work reported in this paper.

Acknowledgements

This work was partially supported by Scientific and Technological Research Council of Turkey (TUBITAK) under contract number of 5189901 and Research Foundation of Turkish Aerospace (No. TM0131). The authors thank to the collaboration between Turkish Aerospace and Bilkent University Institute of Materials Science and Nanotechnology (UNAM). The authors also thank to Enver Kahveci and Mustafa Guler for the assistance in the GIXRD and FIB lithography, respectively.

Appendix A. Supplementary data

Supplementary data to this article can be found online at https://doi.org/10.1016/j.apsusc.2020.147111.

References

[1] K.L. Chopra, S. Major, D.K. Pandya, Transparent conductors-A status review, Thin Solid Films 102 (1983) 1–46.

[2] C. Guillén, J. Herrero, TCO/metal/TCO structures for energy and flexible electronics, Thin Solid Films. 520 (2011) 1–17.
[3] M. Mizuhahsi, Electrical Properties of Vacuum-Deposited Indium Oxide and Indium Tin Oxide Films, Thin Solid Films. 70 (1980) 91–100.
[4] I. Hamberg, C.G. Granqvist, Evaporated Sn-doped In2O3 films: Basic optical properties and applications to energy-efficient windows, J. Appl. Phys. 60 (1986) R123–R159.
[5] R. Bel Hadj Tahar, T. Ban, Y. Ohya, Y. Takahashi, Tin doped indium oxide thin films: Electrical properties, J. Appl. Phys. 83 (1998) 2631–2645.
[6] H. Kim, C.M. Gilmore, A. Piqué, J.S. Horwitz, H. Mattoussi, H. Murata, et al., Electrical, optical, and structural properties of indium-tin-oxide thin films for organic light-emitting devices, J. Appl. Phys. 86 (1999) 6451–6461.
[7] Y.S. Kim, J.H. Park, D.H. Choi, H.S. Jang, J.H. Lee, H.J. Park, et al., ITO/Au/ITO multilayer thin films for transparent conducting electrode applications, Appl. Surf. Sci. 254 (2007) 1524–1527.
[8] C. Guillén, J. Herrero, ITO/metal/ITO multilayer structures based on Ag and Cu metal films for high-performance transparent electrodes, Sol. Energy Mater. Sol. Cells. 92 (2008) 938–941.
[9] J.Y. Lee, J.W. Yang, J.H. Chae, J.H. Park, J.I. Choi, H.J. Park, et al., Dependence of intermediated noble metals on the optical and electrical properties of ITO/metal/ITO multilayers, Opt. Commun. 282 (2009) 2362–2366.
[10] E.N. Cho, P. Moon, C.E. Kim, I. Yun, Modeling and optimization of ITO/Al/ITO multilayer films characteristics using neural network and genetic algorithm, Expert Syst. Appl. 39 (2012) 8885–8889.
[11] D. Kim, Characterization of low pressure annealed ITO/Au/ITO films prepared by reactive magnetron sputtering, J. Alloys Compd. 493 (2010) 208–211.
[12] D. Kim, Low temperature deposition of transparent conducting ITO/Au/ITO films by reactive magnetron sputtering, Appl. Surf. Sci. 256 (2010) 1774–1777.
[13] C.-W. Jeong, C.-H. Shin, D.-I. Kim, J.-H. Chae, Y.-S. Kim, An ITO/Au/ITO Thin Film Gas Sensor for Methanol Detection at Room Temperature, Trans. Electr. Electron. Mater. 11 (2010) 77–80.
[14] S. Thonglem, U. Intatha, K. Pengpat, G. Rujijanagul, T. Tunkasiri, S. Eitssayeam, Electrical and optical properties of ITO/Au/ITO multilayer films for high performance TCO films, Ferroelectrics. 457 (2013) 117–123.
[15] X. Fang, C.L. Mak, J. Dai, K. Li, H. Ye, C.W. Leung, ITO/Au/ITO sandwich structure for Near-infrared plasmonics, ACS Appl. Mater. Interfaces. 6 (2014) 15743–15752.
[16] W. Wei, R. Hong, J. Wang, C. Tao, D. Zhang, Electron-beam irradiation induced optical transmittance enhancement for Au/ITO and ITO/Au/ITO multilayer thin films, J. Mater. Sci. Technol. 33 (2017) 1107–1112.
[17] N. Erdogan, F. Erden, A.T. Astarlioglu, M. Ozdemir, S. Ozbay, G. Aygun, L. Ozyuzer, ITO/Au/ITO multilayer thin films on transparent polycarbonate with enhanced EMI shielding properties, Curr. Appl. Phys. 20 (2020) 489–497.
[18] K.K. Lam, S.M. Ng, H.F. Wong, L. Fei, Y. Liu, K.H. Chan, et al., Effect of thickness on the optical and electrical properties of ITO/Au/ITO sandwich structures, ACS Appl. Mater. Interfaces. 12 (2020) 13437–13446.
[19] H.S. Im, S.K. Kim, T.J. Lee, T.Y. Seong, Combined effects of oxygen pressures and RF powers on the electrical characteristics of ITO-based multilayer transparent electrodes, Vacuum. 169 (2019) 108871.
[20] N.R. Armstrong, C. Carter, C. Donley, A. Simmonds, P. Lee, M. Brumbach, et al., Interface modification of ITO thin films: Organic photovoltaic cells, Thin Solid Films. 445 (2003) 342–352.
[21] W.J. Dong, J.Y. Park, J. Ham, G.H. Jung, I. Lee, J.L. Lee, Dual Effect of ITO-Interlayer on Inverted Top-Illuminated Polymer Solar Cells: Wetting of Polyelectrolyte and Tuning of Cavity, Adv. Funct. Mater. 26 (2016) 5437–5446.
[22] J.S. Kim, R.H. Friend, F. Cacialli, Surface energy and polarity of treated indium-tin-oxide anodes for polymer light-emitting diodes studied by contact-angle measurements, J. Appl. Phys. 86 (1999) 2774–2778.
[23] S. Besbes, H. Ben Ouada, J. Davenas, L. Ponsonnet, N. Jaffrezic, P. Alcouffe, Effect of surface treatment and functionalization on the ITO properties for OLEDs, Mater. Sci. Eng. C. 26 (2006) 505–510.
[24] Z.Z. You, J.Y. Dong, Surface modifications of ITO electrodes for polymer light-emitting devices, Appl. Surf. Sci. 253 (2006) 2102–2107.
[25] M.H. Jung, H.S. Choi, Surface treatment and characterization of ITO thin films using atmospheric pressure plasma for organic light emitting diodes, J. Colloid Interface Sci. 310 (2007) 550–558.
[26] J. Davenas, S. Besbes, A. Abderrahmen, N. Jaffrezic, H. Ben Ouada, Surface characterisation and functionalisation of indium tin oxide anodes for improvement of charge injection in organic light emitting diodes, Thin Solid Films. 516 (2008) 1341–1344.
[27] A. Arazna, G. Koziol, K. Janeczek, K. Futera, W. Stęplewski, Investigation of surface properties of treated ITO substrates for organic light-emitting devices, J. Mater. Sci. Mater. Electron. 24 (2013) 267–271.
[28] S.G. Jung, K.B. Choi, C.H. Park, Y.S. Shim, C.H. Park, Y.W. Park, et al., Effects of Cl2 plasma treatment on stability, wettability, and electrical properties of ITO for OLEDs, Opt. Mater. 93 (2019) 51–57.
[29] M. Shekargoftar, R. Krumpolec, T. Homola, Enhancement of electrical properties of flexible ITO/PET by atmospheric pressure roll-to-roll plasma, Mater. Sci. Semicond. Process. 75 (2018) 95–102.
[30] H.K. Park, S.W. Yoon, W.W. Chung, B.K. Min, Y.R. Do, Fabrication and characterization of large-scale multifunctional transparent ITO nanorod films, J. Mater. Chem. A. 1 (2013) 5860–5867.
[31] N. Gupta, S. Sasikala, D.B. Mahadik, A.V. Rao, H.C. Barshilia, Dual-scale rough multifunctional superhydrophobic ITO coatings prepared by air annealing of sputtered indium-tin alloy thin films, Appl. Surf. Sci. 258 (2012) 9723–9731.
[32] H.Y. Erbil, Surface Chemistry of Solid and Liquid Interfaces, Blackwell Publishing, Oxford, 2006.
[33] H.Y. Erbil, The debate on the dependence of apparent contact angles on drop contact area or three-phase contact line: A review, Surf. Sci. Rep. 69 (2014) 325–365.
[34] C. Ozcan, N. Hasirci, Evaluation of Surface Free Energy for PMMA Films, J. Appl. Polym. Sci. 108 (2008) 438–446.
[35] C.C. Ho, M.C. Khew, Surface free energy analysis of natural and modified natural rubber latex films by contact angle method, Langmuir. 16 (2000) 1407–1414.
[36] S.K. So, W.K. Choi, C.H. Cheng, L.M. Leung, C.F. Kwong, Surface preparation and characterization of indium tin oxide substrates for organic electroluminescent devices, Appl. Phys. A Mater. Sci. Process. 68 (1999) 447–450.
[37] S. Vunnam, K. Ankireddy, J. Kellar, W. Cross, Surface modification of indium tin oxide for direct writing of silver nanoparticulate ink micropatterns, Thin Solid Films. 531 (2013) 294–301.
[38] Z. Zhong, S. Yin, C. Liu, Y. Zhong, W. Zhang, D. Shi, et al., Surface energy for electroluminescent polymers and indium-tin-oxide, Appl. Surf. Sci. 207 (2003) 183–189.
[39] S. Elmas, S. Korkmaz, S. Pat, Investigation of physical properties and surface free energy of produced ITO thin films by TVA technique, J. Mater. Sci. Mater. Electron. 30 (2019) 8876–8882.
[40] C.D. Volpe, S. Siboni, Some reflections on acid-base solid surface free energy theories, J. Colloid Interface Sci. 195 (1997) 121–136.
[41] D.Y. Kwok, The usefulness of the Lifshitz–van der Waals/acid–base approach for surface tension components and interfacial tensions, Colloids Surfaces A Physicochem. Eng. Asp. 156 (1999) 191–200.
[42] D.Y. Kwok, A.W. Neumann, Contact angle measurement and contact angle interpretation, Adv. Colloid Interface Sci. 81 (1999) 167–249.
[43] D.Y. Kwok, A.W. Neumann, Contact angle interpretation in terms of solid surface tension, Colloids Surfaces A Physicochem. Eng. Asp. 161 (2000) 31–48.
[44] C.D. Volpe, S. Siboni, Acid–base surface free energies of solids and the definition of scales in the Good–van Oss-Chaudhury theory, J. Adhes. Sci. Technol. 14 (2000) 235–272.
[45] C.D. Volpe, S. Siboni, Troubleshooting of surface free energy acid-base theory applied to solid surfaces: The case of Good, van Oss and Chaudhury theory, in: K.L. Mittal (Ed.), Acid-Base Reactions: Relevance to Adhesion Science and Technology, vol. 2, VSP, New York, 2000, pp. 55–90.
[46] C.D. Volpe, D. Maniglio, S. Siboni, M. Morra, Recent theoretical and experimental advancements in the application of van Oss–Chaudury–Good acid–base theory to the analysis of polymer surfaces I. General aspects, J. Adhes. Sci. Technol. 17 (2003) 1477–1505.
[47] C.D. Volpe, S. Siboni, D. Maniglio, M. Morra, C. Cassinelli, M. Anderle, G. Speranza, R. Canteri, C. Pederzolli, G. Gottardi, S. Janikowska, A. Lui, Recent theoretical and experimental advancements in the application of the van Oss–Chaudhury–Good acid–base theory to the analysis of polymer surfaces II. Some peculiar cases, J. Adhes. Sci. Technol. 17 (2003) 1425–1456.
[48] C.D. Volpe, D. Maniglio, M. Brugnara, S. Siboni, M. Morra, The solid surface free energy calculation I. In defense of the multicomponent approach, J. Colloid Interface Sci. 271 (2004) 434–453.
[49] S. Sibonio, C.D. Volpe, On the definition of scales in van Oss–Chaudhury-Good acid–base theory, MATCH Commun. Math. Comput. Chem. 56 (2006) 291–316.
[50] A. Hofrichter, P. Bulkin, B. Drevillon, Plasma treatment of polycarbonate for improved adhesion, J. Vac. Sci. Technol. A. 20 (2002) 245–250.
[51] H. Yaghoubi, N. Taghavinia, Surface chemistry of atmospheric plasma modified polycarbonate substrates, Appl. Surf. Sci. 257 (2011) 9836–9839.
[52] X. Zhang, Y. Zhong, X. Zhang, L. Li, Y. Yan, Plasma and chromic acid treatments of polycarbonate surface to improve coating-substrate adhesion, Surf. Interface Anal. 45 (2013) 1893–1898.
[53] N. Bhatnagar, Plasma Surface Treatment to Enhance Adhesive Bonding, in: A. Pizzi, K.L. Mittal (Eds.), Handb, CRC Press, Adhes. Technol., 2017, pp. 67–94.
[54] D.K. Owens, R.C. Wendt, Estimation of the surface free energy of polymers, J. Appl. Polym. Sci. 13 (1969) 1741–1747.
[55] S. Wu, Calculation of interfacial tension in polymer systems, J. Polym. Sci. Part C Polym. Symp. 34 (1971) 19–30.
[56] C.J. Van Oss, M.K. Chaudhury, R.J. Good, Interfacial Lifshitz-van der Waals and polar interactions in macroscopic systems, Chem. Rev. 88 (1988) 927–941.
[57] H.W. Fox, W.A. Zisman, The Spreading of Liquids on Low Energy Surfaces. I. Polytetrafluoroethylene, J. Colloid Sci. 5 (1950) 514–531.
[58] H.W. Fox, W.A. Zisman, The Spreading of Liquids on Low-Energy Surfaces. II. Modified Tetrafluoroethylene Polymers, J. Colloid Sci. 7 (1952) 109–121.
[59] H.W. Fox, W.A. Zisman, The spreading of liquids on low-energy surfaces. III. Hydrocarbon surfaces, J. Colloid Sci. 7 (1952) 428–442.
[60] S. Siboni, C.D. Volpe, D. Maniglio, M. Brugnara, The solid surface free energy calculation II. The limits of the Zisman and of the “equation-of-state” approaches, J. Colloid Interface Sci. 271 (2004) 454–472.
[61] O. Tuna, Y. Selamet, G. Aygun, L. Ozyuzer, High quality ITO thin films grown by dc and RF sputtering without oxygen, J. Phys. D. Appl. Phys. 43 (2010) 055402.
[62] C.J. Van Oss, R.F. Giese, Z. Li, K. Murphy, J. Norris, M.K. Chaudhury, et al., Determination of contact angles and pore sizes of porous media by column and thin layer wicking, J. Adhes. Sci. Technol. 6 (1992) 413–428.
[63] H.Y. Erbil, Calculation of Spreading pressure from Contact Angle Data on Polymer Surfaces, Langmuir. 10 (1994) 2006–2009.
[64] R.J. Good, Contact angle, wetting and adhesion: a critical review, J. Adhes. Sci. Technol. 6 (1992) 1269–1302.
[65] J. Lai, B. Sunderland, J. Xue, S. Yan, W. Zhao, M. Folkard, et al., Study on hydrophilicity of polymer surfaces improved by plasma treatment, Appl. Surf. Sci. 252 (2006) 3375–3379.
[66] T. Murakami, S. ichi Kuroda, Z. Osawa, Dynamics of polymeric solid surfaces

treated with oxygen plasma: Effect of aging media after plasma treatment, J. Colloid Interface Sci. 202 (1998) 37–44.
[67] S. Ozbay, H.Y. Erbil, Superhydrophobic and oleophobic surfaces obtained by graft copolymerization of perfluoroalkyl ethyl acrylate onto SBR rubber, Colloids Surfaces A Physicochem. Eng. Asp. 481 (2015) 537–546.
[68] S. Ozbay, H.Y. Erbil, Solution copolymerization of perfluoroalkyl ethyl methacrylate with methyl methacrylate and butyl acrylate: Synthesis and surface properties, Colloids Surfaces A Physicochem. Eng. Asp. 452 (2014) 9–17.
[69] J. Tamarit-Lopez, S. Morais, R. Puchades, A. Maquieira, Oxygen plasma treated interactive polycarbonate DNA microarraying platform, Bioconjug. Chem. 22 (2011) 2573–2580.
[70] J. Kelar, M. Shekargoftar, R. Krumpolec, T. Homola, Activation of polycarbonate (PC) surfaces by atmospheric pressure plasma in ambient air, Polym. Test. 67 (2018) 428–434.
[71] L.J. Meng, M.P. Dos Santos, Properties of indium tin oxide films prepared by rf reactive magnetron sputtering at different substrate temperature, Thin Solid Films 322 (1998) 56–62.